Internship Report: FRC RMF heating at a 1 keV scale

Libby Tolman, advised by Professor Sam Cohen

September 14, 2014

Contents

1 Introduction

The field-reversed configuration (FRC) device is a long cylindrical tube with a strong axial magnetic field. This device may be capable of playing host to fusion reactions in a way that is simple, clean, and small-scale, giving it the potential to one day be an effective fusion reactor for niche applications. On top of the strong axial magnetic field, in the FRC rotating magnetic fields are used to create a plasma current in the center of the device, which reverses the direction of the field in certain regions, creating an ellipsoidal confinement structure which may be similar to the configuration pictured in Figure 1. This overall confinement structure can be much smaller than that of other fusion devices like tokamaks, because classical transport, the baseline moder

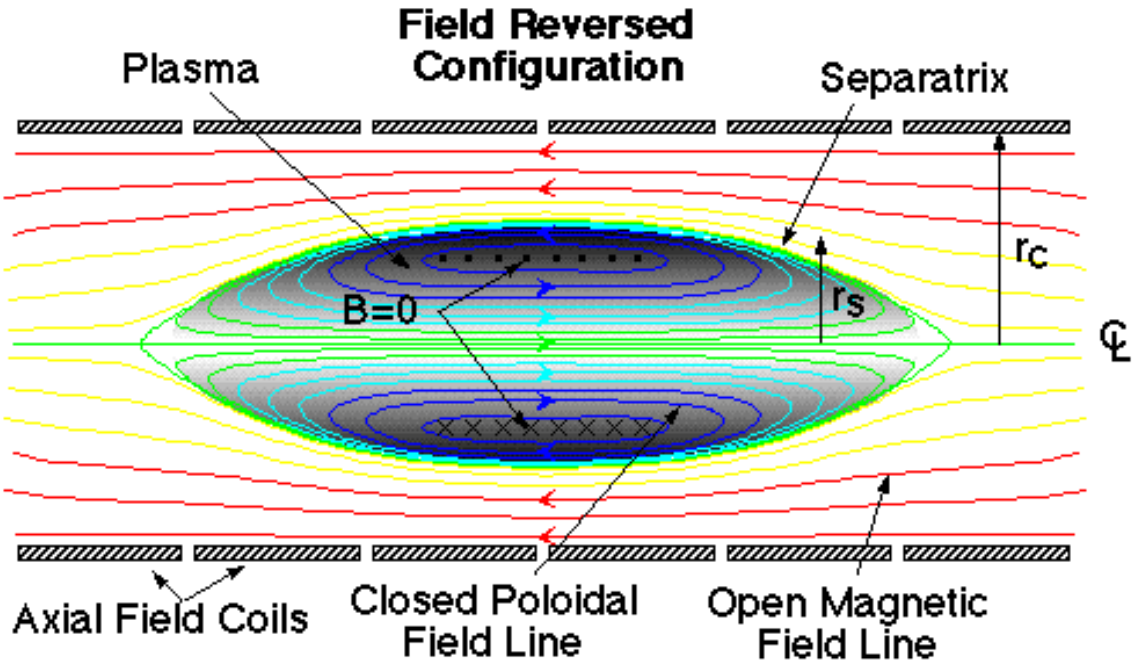

Figure 1: The FRC confinement structure, from depts.washington.edu/rppl/images/frcintropict.gif.

for FRC's, is about 10 times slower than neoclassical transport, the baseline mode for toroidal devices.

At PPPL, the experiment to investigate the physics and engineering of the FRC is the PFRC project. This project plans to have four stages of devices, PFRC-1, PFRC-2, PFRC-3, and PFRC-4, each demonstrating more refined and advanced technologies. The PFRC has at least three characteristics which make it unique among other present and historical FRC experiments. First, PFRC devices use odd parity rotating magnetic fields instead of even parity ones, a choice which is speculated to improve confinement. Second, the PFRC will use ^{3}He as a fuel. The ^{2}D + ^{3}He $\rightarrow$ ^{4}He + ^{1}p + 18.3 MeV reaction is projected to reduce neutron production in comparison to deutrerium-tritium fuels, which can improve reactor safety and durability. Finally, the PFRC aims to heat ions using the same rotating magnetic fields that drive the plasma current which creates confinement in the first place. Other experiments have used neutral beams to heat the plasma, but PFRC has rejected this technique because it involves large and expensive equipment.

The goal of this paper is to introduce those working on the PFRC to the ideas and techniques relevant to heating by RMF to 1 keV which were relevant to this summer's internship, suggest papers to reference, and to suggest directions for future study. In designing an RMF heating system, two parameters which must be selected are the RMF frequency and strength, so particular attention is paid to these two qualities. The heating target envisioned throughout the paper is 1 keV, since heating ions to this average temperature would serve as a proof of concept of the viability of RMF as a heating method. A functioning reactor burning D-He^3 fuel would require ion temperatures around 100 keV.

The paper proceeds by first considering the macroscopic context of RMF heating: Without any knowledge of the mechanism of RMF ion heating, it is yet possible to understand some constraints affecting field frequency and strength, and the limits that each of these parameters places on the amount of energy that can be delivered to the plasma. The second section of the

paper delves into the form of the RMF fields, how they cause individual ions to gain energy, how this interaction is influenced by plasma and field characteristics, and the tools that are used to study these phenomena. This section also suggests directions for future study. The third section presents the results of Hamiltonian code simulations designed to quantitatively suggest how frequency and field strength influence the heating of an FRC plasma. The code used to conduct the analyses in the paper may be obtained from Professor Cohen or Libby Tolman.

2 RMF heating from a macroscopic view

The nature of any heating that RMF causes in an FRC will ultimately be determined by how the fields interact with individual plasma particles, and how these particles interact with each other. Before considering these specifics, however, it is useful to study the setup of the PFRC-2 experiment from a large-scale view, as this both creates a context for further, more detailed study, and allows the determination certain limitations on the frequency and the strength of the field and on the magnitude and speed of the heating. Much of the material that follows is inspired by information in [2], and this paper can be turned to for more information.

2.1 RMF Frequency

The PFRC confines its plasma in a polycarbonate vacuum vessel. This vacuum vessel is enclosed by a set of RF antennas which deliver the RMF. These RF antennas are elements of a circuit; in this circuit the antennas play the role of an inductor: a changing electric current flows through their coils, and these coils resist this change in a manner determined by their configuration and by the nature of the plasma that fills them. The rest of the circuit contains the elements documented in [1].

These elements may be represented schematically as in Figure 2. The inductor is the RF setup; the resistor and capacitors come from other elements of the PFRC circuit. Together, these elements form an RLC circuit. Such a circuit is characterized by a resonant frequency $\omega_R = \frac{1}{\sqrt{LC}}$. At this frequency, the impedance of the circuit is due only to the resistor, because the tendency of the inductor to pass low frequencies and the tendency of the capacitors to pass high frequencies exactly cancel. At this frequency, the amount of current the circuit passes is maximized, and, because the energy stored in an inductor goes as current squared, the amount of energy stored in the RF coils is maximized as well.

Since the energy in the RF coils heats the ions and drives current, a preliminary view suggests that the coils' ability to perform these functions might be maximized when the energy stored in the coils is as well. This approach is indeed used to guide the selection of frequencies used to run FRC experiments. However, finding this resonant frequency is not trivial, as the inductance L of the RMF coils depends on the characteristics of the plasma that fills it. As explained in [1], when there is no plasma in the coils, the inductance of the coils is simply determined by their geometrical configuration. However, plasma may shield parts of the interior of the coils from magnetic field, reducing the magnetic flux caused by a given current in the coils and accordingly reducing the inductance. Some theoretical studies of this phenomenon in even parity FRCs ([4]) suggest that sufficiently strong magnetic fields will nearly fully penetrate the reactor after a time on the order of tens of microseconds for small, cool FRCs.

Equivalent theoretical studies have not been done on odd parity FRCs, so exploration of magnetic field penetration and the corresponding resonant frequency shift have been experi-

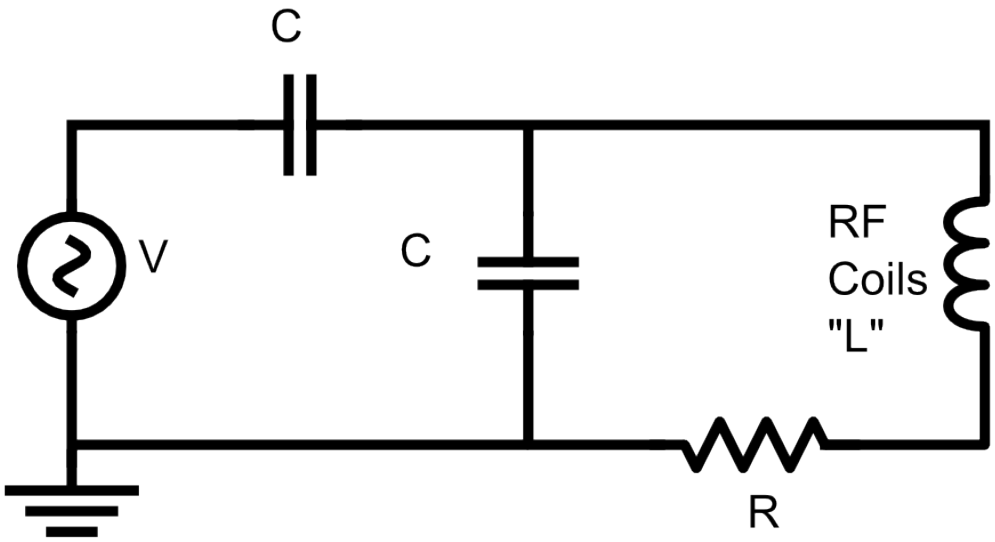

Figure 2: A simplified schematic of the PFRC circuit.

mental. These studies are done by measuring the ratio input rf power to reflected power, a measure of distance from resonance, at different frequencies. Results are found in [2].

The sensitivity of the system to the frequency selection is very important: Though we will see later that a given resonant frequency may not be the best frequency for moving ions and electrons on a microscopic level, far from the resonant frequency there will be barely any strength in the FRC fields, rendering them incapable of providing heat or current. Thus, for a given inductance and capacitance we would like to know how far the frequency may be adjusted in order to improve the heating characteristics.

This is measured by Q, the ratio of the resonant frequency to the bandwidth of the circuit at half of its resonant power. Work in [2] has found values of Q from around 60 to 200 in the PFRC-2 at a resonant frequency of 8 MHz in the absence of plasma; when plasmas exist, this value of Q decreases by 10% to 70%. Considering an intermediate value Q = 100 as an example, one could adjust the RMF frequency in the range f = 8 MHz ± .04 MHz and still obtain good power in the fields.

Later in this writeup, we will learn that RMF frequencies close to the ion cyclotron frequency are beneficial for heating. In a magnetic field of 1000 G, a typical value which might be encountered in the PFRC-2, this frequency is

$$f_c = \frac{eB}{2\pi mc} = 1.52 \text{ MHz}, \tag{1}$$

significantly below the present range in frequency that gives good energy in the fields for the device as currently configured. This is because the device is currently designed to optimize

current drive, which requires high frequencies. In future devices, this conflict may be resolved by increasing the strength of the axial field, which could increase the ion cyclotron frequency into a range which is good for both current and heating.

2.2 RMF field strength

The strength of the voltage used to run the RMF antenna and the frequency of this voltage will determine the strength of the magnetic fields that actually penetrate the plasma. The strength of these fields controls the amount of energy that may be delivered to the plasma.

In particular, consider the confined, ellipsoidal region in Figure 1. The energy stored in the fields in this region is given by

$$U = \int dV \frac{B^2}{8\pi}, \tag{2}$$

and this energy represents the energy that may be delivered to the particles. As explained in the second section, the form of the RMF magnetic fields may be modeled by the following equations:

$$B_r = 2B_{RMF}\left[I_0\left(kr\right) - \frac{I_1\left(kr\right)}{kr}\right]\sin\left(kz\right)\cos\left(\phi - \phi_0 - \omega t\right), \tag{3}$$

$$B_\phi = 2B_{RMF}\frac{I_1(kr)}{kr}\sin\left(kz\right)\sin\left(\phi - \phi_0 - \omega t\right), \tag{4}$$

and

$$B_z = 2B_{RMF}I_1(kr)\cos\left(kz\right)\cos\left(\phi - \phi_0 - \omega t\right). \tag{5}$$

Inserting these into (2) evaluated over the confined region gives

$$U = \int_0^{2\pi} d\phi \int_0^{r_s} r dr \int_{-z_s\sqrt{1-\frac{r^2}{r_s^2}}}^{z_s\sqrt{1-\frac{r^2}{r_s^2}}} dz \frac{B_r^2 + B_\phi^2 + B_z^2}{8\pi}. \tag{6}$$

This expression numerically integrated in Python with parameters $r_s = 7$ cm, $z_s = 28$ cm and $k = \frac{\pi}{2z_s}$ at $t = 0$ gives 446.8 cm$^3 B_{RMF}^2$ as the amount of the energy stored in the fields.

This figure may be compared to the amount of energy necessary to raise the average energy of ions in an FRC plasma by a given amount ΔE_i, represented by

$$E = \int n_i \Delta E_i dV, \tag{7}$$

where n_i is the volume density of the ions and the volume integral runs over the region of the FRC in which is plasma is confined. In the PFRC experiment, a typical starting ion density might be $n_i = 10^{11}$ cm^{-3}, which would eventually be raised to $n_i = 10^{13}$ cm^{-3}, while a starting goal for ion heating is $\Delta E = 1$ keV. The relevant region is then the ellipsoid with semi-principal axes r_s, r_s, and z_s with volume $V = \frac{4}{3}\pi r_s^2 z_s$. For PFRC parameters, $r_s = 7$ cm, $z_s = 28$ cm, the integral then gives $E = 5.75 \times 10^{17}$ eV $= 9.21 \times 10^5$ ergs.

Suppose that an experiment wanted to reach the heating goal in Δt seconds. The required heating power would then be $P = \frac{9.21\times10^5}{\Delta t}$ ergs per second, and the RMF fields would have to deposit their strength every $\frac{446.8\text{cm}^3 B_{RMF}^2 \Delta t}{9.21\times10^5\text{ergs}}$ seconds. Increasing the strength of the field will decrease the demands on the mechanism responsible for transferring energy from the fields to the particles.

We have thus reviewed the heating trends discernible from a high level view of heating. Next remains to understand the mechanism that transfers energy from the fields to the particles.

3 RMF heating from a microscopic view

As ions move in the FRC, they experience rotating magnetic fields which induce electric fields. These electric fields will cause their energy to change at the rate $\frac{dH}{dt} = q_i \vec{E} \cdot \vec{v}$. This energy change is predicted to increase the energy of the ions in the FRC in a way that may be classified as heating. To understand this process, we first need to understand the nature of the fields that cause the heating.

3.1 Nature of RMF fields

The PFRC uses odd parity RMF fields, commonly called RMF_0 when the possibility of confusion with even parity RMF fields exists. These fields are formed from a set of rf antennas shown schematically in Figure 3, which receive rf signals. The signal flowing to the coils shown in red

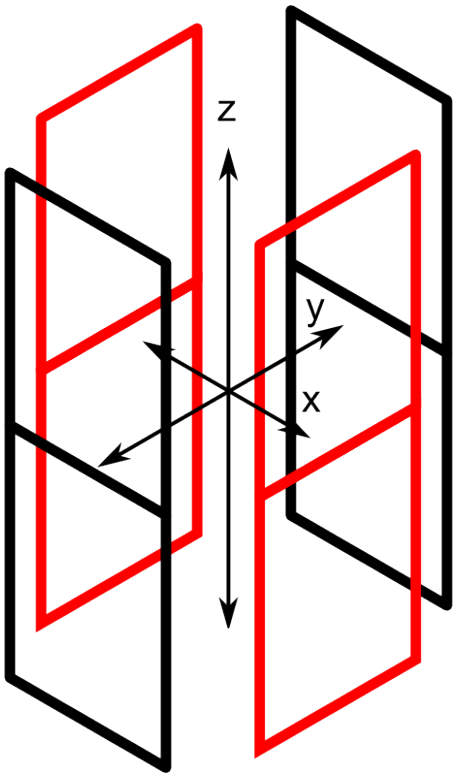

Figure 3: Schematic representation of FRC RMF coils.

in the diagram is ninety degrees out of phase with the signal flowing to the coils in black, which creates fields interior to the coils which rotate. These fields are modeled by the following vector

potential:

$$A_r = \frac{2B_{RMF}}{k} I_0(\xi) \cos(kz) \sin(\psi), \tag{8}$$

$$A_\phi = \frac{2B_{RMF}}{k} I_0(\xi) \cos(kz) \cos(\psi), \tag{9}$$

and

$$A_z = -\frac{2B_{RMF}}{k} I_1(\xi) \sin(kz) \sin(\psi), \tag{10}$$

where $\xi \equiv k\sqrt{x^2+y^2}$, $\psi \equiv \arctan(y/x) - \omega t$, and ω is the frequency of the RMF, whence the magnetic fields are found via $\vec{B} = \nabla \times \vec{A}$. A cross section of these fields is shown in Figure 4. More detailed three dimensional modeling of the fields is the subject of work by Matt Lotaki.

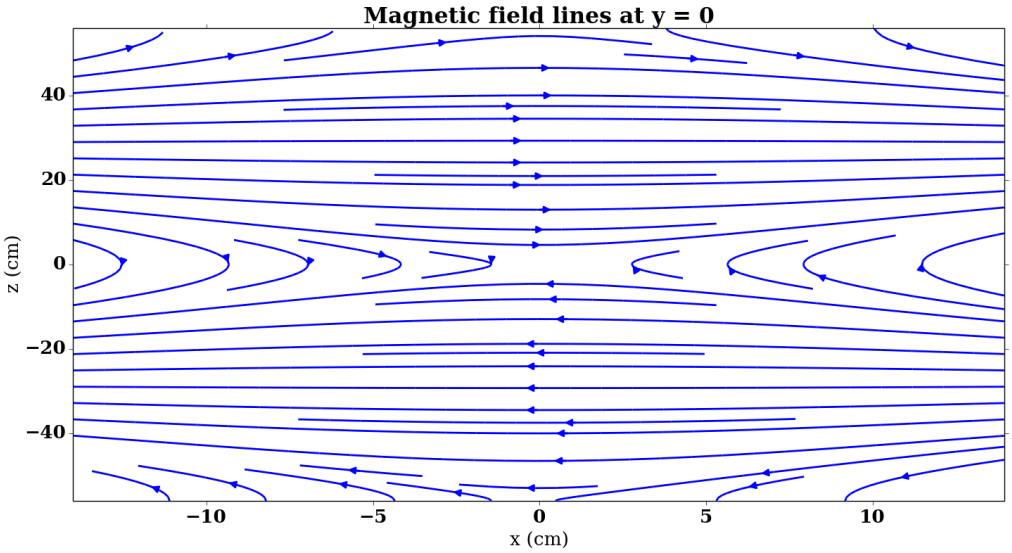

Figure 4: Cross section of fields created by (8) through (10), with parameters $r_s = 7$ cm, $z_s = 28$ cm, and k = $\frac{\pi}{2z_s}$.

The electric fields induced by this RMF are predicted to drive currents which create a confining magnetic field structure and to heat ions, so ideally they would be maintained throughout the operation of the reactor. However, materials constraints in current experiments hinder constant operation of the fields. In particular, as [1] notes, in the PFRC-2, certain elements of the machine melt if the RMF is maintained for too long. To deal with this issue, the machine is run in a pulsed mode. The RMF is turned on for a time ranging from .1 to 15 ms, then turned off again. This process is repeated ad nauseam; the ratio of time on to time off results in a duty factor around .5%. Visually, this process results in a series of bright flashes coming from a dim purple plasma.

3.2 Confinement predicted from RMF fields

Every time the RMF is turned on, the currents it drives modify the structure of the axial magnetic field that is constantly maintained in the device. The precise form of this modification of structure needs more experimental investigation. However, for theoretical studies of confinement and heating, the resulting magnetic field structure is modeled as a Hill Vortex, a structure

which is chosen for its tractability to calculation. The Hill Vortex has vector potential

$$\psi(r,z) = rA_\phi = \psi_0 \left(\frac{r^2}{r_s^2}\right)\left(1 - \frac{r^2}{r_s^2} - \frac{z^2}{z_s^2}\right), \tag{11}$$

where $\psi_0 \equiv \frac{B_0 r_s^2}{2}$, so that

$$B = \frac{\psi_0}{r_s^2}\left[\hat{r}\left(\frac{-2zr}{z_s^2}\right) + \hat{z}\left(2 - \frac{4r^2}{r_s^2} - \frac{2z^2}{z_s^2}\right)\right]. \tag{12}$$

Such magnetic fields are illustrated by the common FRC image in Figure 5.

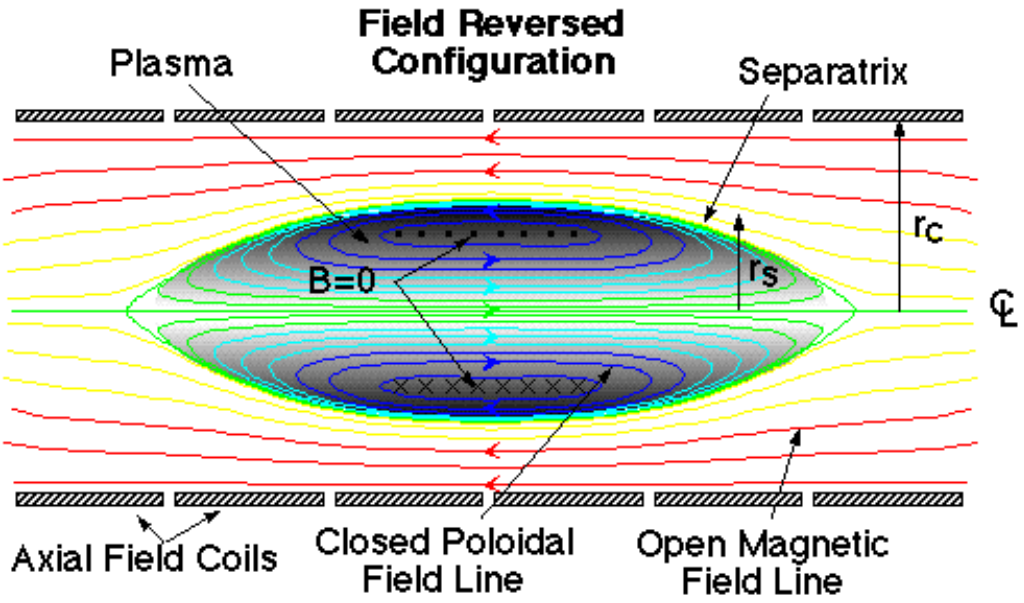

Figure 5: FRC fields, from http://depts.washington.edu/rppl/images/frcintropict.gif.

This magnetic field structure confines ions. The Lagrangian for particle motion in this magnetic field is

$$L = \frac{m}{2}\left(\dot{r}^2 + r^2\dot{\phi}^2 + \dot{z}^2\right) + \frac{qr}{c}\dot{\phi}A_\phi, \tag{13}$$

which yields a Hamiltonian of

$$H = \frac{1}{2m}\left[p_r^2 + p_z^2 + \frac{1}{r^2}\left(p_\phi - \frac{q\psi}{c}\right)^2\right], \tag{14}$$

where the p correspond to canonical momenta, so for example $p_\phi = mr^2\dot{\phi} + \frac{qrA_\phi}{c}$.

This does not depend on ϕ, (the flux function depends on r and z only), so the particle's r and z motion is governed by an effective potential,

$$V_{eff} = \frac{1}{2mr^2}\left(p_\phi - \frac{q}{c}\psi\right)^2. \tag{15}$$

A plot of an example of this effective potential in the FRC midplane (where z = 0) is shown in Figure 6. It clearly takes the form of a well, which will prevent particles from going too far from or too close to the axis of the FRC. Physically, this happens because the midplane axial

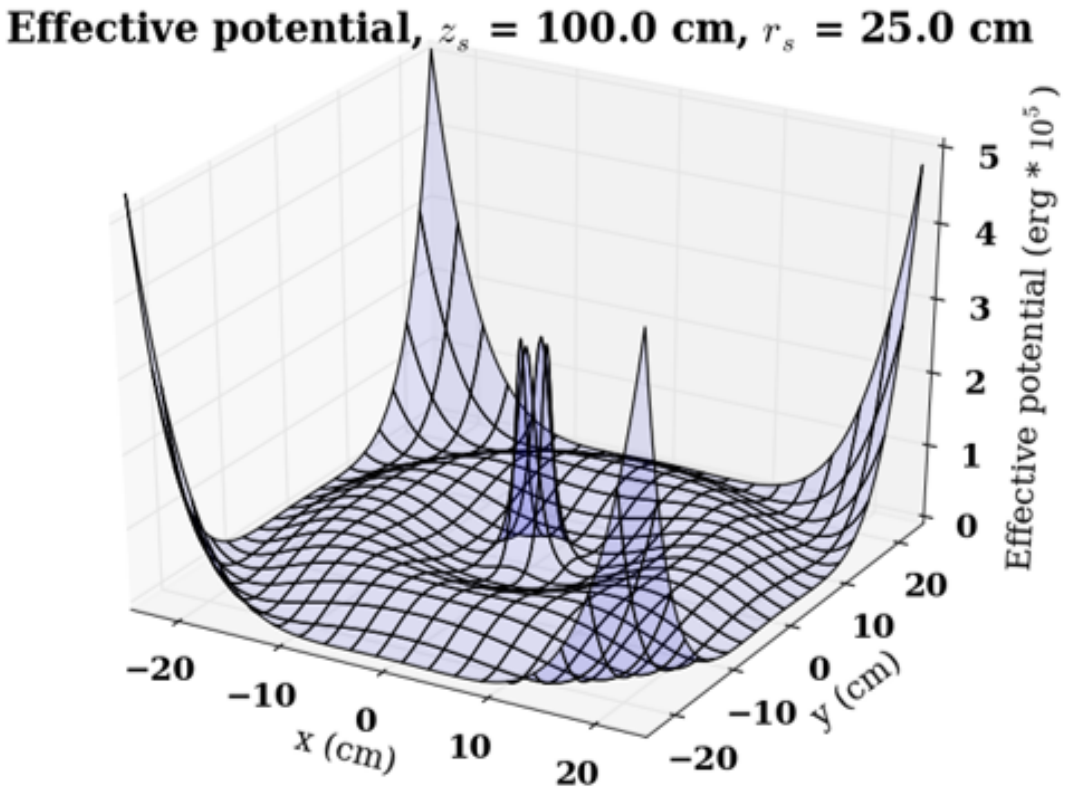

Figure 6: An example confining effective potential in the midplane.

fields in the FRC increase in strength near the center of the device and far from the center of the device; such magnetic fields impede motion across themselves.

The Hill Vortex will also confine particles moving in certain directions when they leave the midplane. This can be seen by explicit calculation, as done in [5], or from a physical argument. This proceeds as outlined in Figure 12: A particle with positive angular velocity, shown on the left, will get turned back towards the midplane by the magnetic fields it encounters traveling away from the midplane, while a particle with negative angular velocity will get pushed away.

3.3 Ion motion under confinement

Ion motion in the FRC confinement structure just described takes a variety of different shapes, which depend on the particle's initial velocity, position, and mass. Detailed description of these orbits is presented in [5], as well as other work by Cohen and Landsman. In general, orbits in the midplane take three shapes. The first is a cyclotron orbit, typical of particles located in strong magnetic fields, either very near the axis of the device or far from it, which do not have enough energy to escape this region. A midplane cyclotron orbit is pictured in Figure 8 in its effective potential. Since the cyclotron orbit moves clockwise, as seen in the figure, it is unstable to perturbations, and will not return to the midplane after it leaves. An example of this phenomenon is seen in Figure 9, in which a perturbed cyclotron orbit leaves the midplane and becomes chaotic. This loss of order corresponds to a loss of confinement. We will see later that many cyclotron orbits are difficult to heat, so this escape from the Hill Vortex may in fact be a positive characteristic: with difficult-to-heat cyclotron particles removed, the remaining

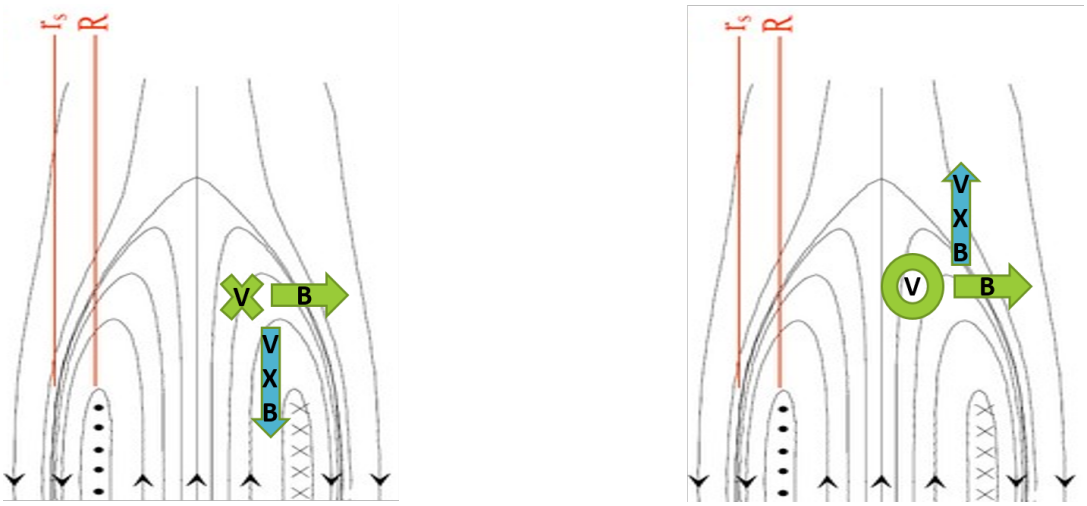

Figure 7: Forces acting on particle leaving the midplane; underlying FRC image from www.aa.washington.edu/research/plasmaDynamics/images/FRCcrosssection.jpg.

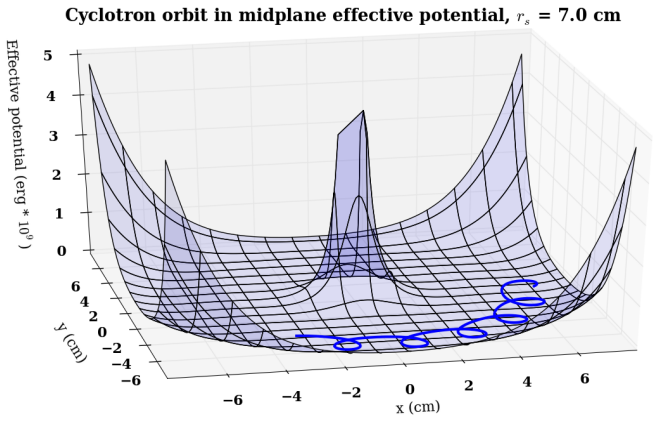

Figure 8: A cyclotron orbit, with initial particle energy 5 eV and initial radius = 6.435 cm (r_s = 7 cm).

particles may be easier to heat up, allowing the overall machine to experience good energy gain.

A second type of orbit is a figure 8 orbit, shown in Figure 10. This orbit is typical of particles with high velocities away from the center of the device which allow them to traverse in and out of their potential well. Figure 8 orbits may move in either direction, so unlike a cyclotron orbit, they can be both stable an unstable to displacement away from the midplane; an example of a stable figure 8 orbit is shown in Figure 11.

The third major type of orbit is the betatron orbit, which is typical of particles located near the point in the FRC with no magnetic field that have high enough velocity around the FRC to make comparatively small excursions radially. Such orbits always go around the device in the stable direction; an example preturbed orbit is shown in Figure 13.

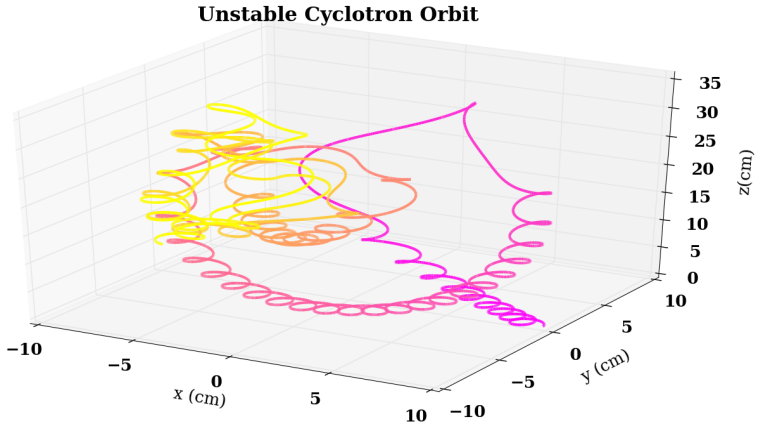

Figure 9: Path taken by a cyclotron orbit that leaves the midplane.

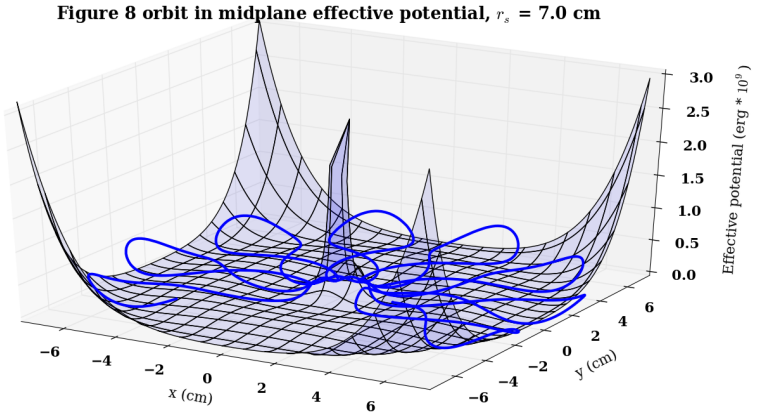

Figure 10: A figure 8 orbit, with initial particle energy 100 eV and initial radius = 1.98 cm (r_s = 7 cm)

3.4 Ion motion before confinement

It is thus possible to gain good understanding of ion motion under confinement in the Hill Vortex. As a side note, it might be interesting for future researchers to understand how the *formation* of this field structure modifies the ion distribution.

Simulations described in [6] suggest the formation of the field reversed configuration takes on the order of 2 μs. While this time period is a short fraction of milliseconds for which an experimental burst of RMF might last, it is a significant fraction of the roughly 5 μs for which a PIC code simulation of particle behavior might run, and this is a timescale which will be of particular interest in the final section of this paper.

We already know that the characterisics of an ion's motion will influence its ability to stay confined; we will see later that the amount of energy that a particle gains from RMF as a

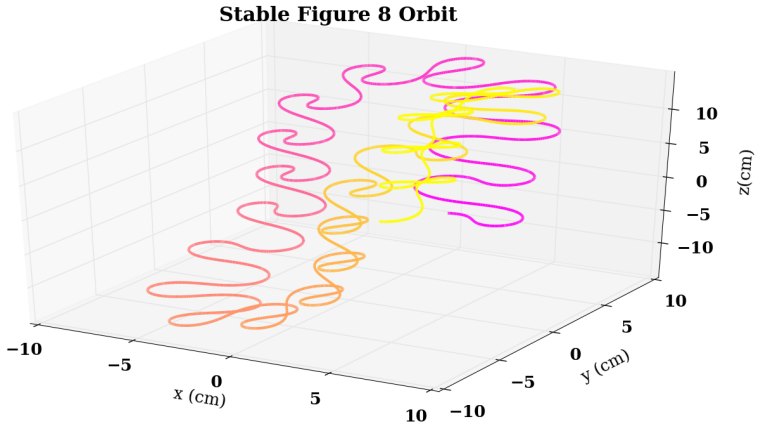

Figure 11: Path taken by a stable figure-8 orbit that leaves the midplane.

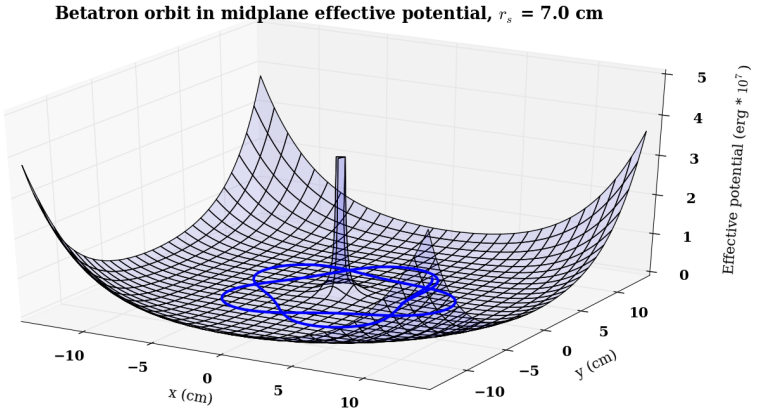

Figure 12: A betatron orbit, with initial particle energy 5 eV and initial radius = 4.455 cm (r_s = 7 cm)

heating mechanism also depends very much on the nature of the ion orbit as well. Thus, if the formation of the confinement structure tended to move ions to positions and velocities corresponding to certain types of orbits and not to others, this could significantly influence the heating of the ions.

3.5 Ion response to RMF while confined

As ions move in the orbits determined by their Hill vortex confinement, they are in addition subjected to rotating magnetic fields and the rotating electric fields that they induce. The vector potential of these fields modeled by (8) through (10).

Ion response to these fields is best understood through numerical simulations of ion motion and energy. This project used the code RMF version 2.00, a Hamiltonian code created by Alan

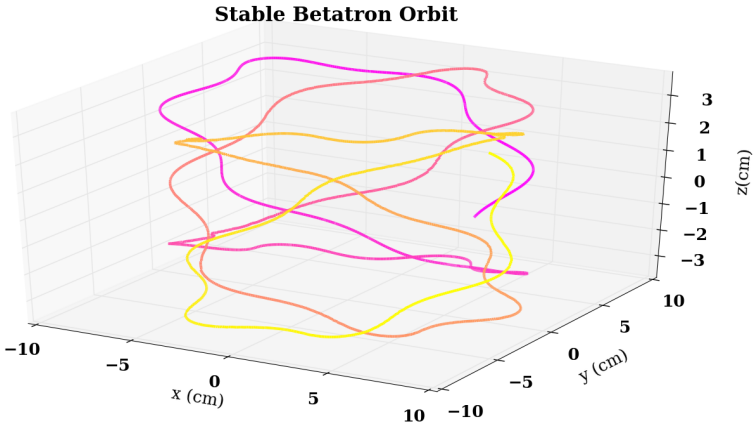

;

Figure 13: Path taken by a betatron orbit that leaves the midplane.

Glasser of Los Alamos National Laboratory, to follow the path of individual particles as they move through the FRC.

In RMF, a particle's initial position and velocity are specified in terms of five variables: its initial energy, its initial radial position, its initial z position, and two angles θ and ϕ, described in Figure 14. From these initial conditions, the program evolves the particle through a user-

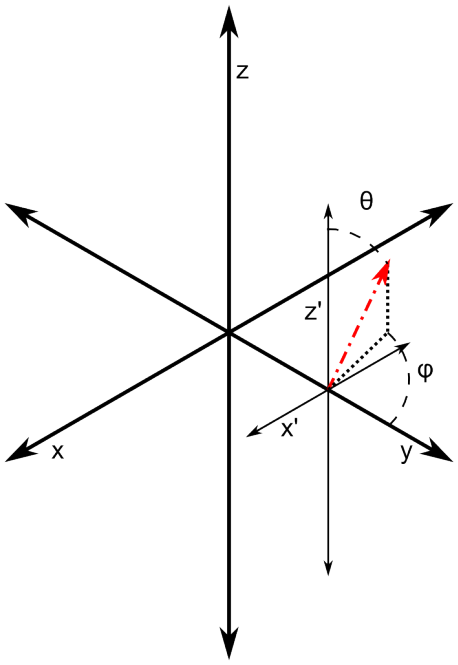

Figure 14: The angles used to specify initial particle velocity. The unprimed axes are centered on the middle of the device, while the primed ones are centered on the particle's position. The red arrow is the particle's velocity.

specified number of time steps and returns the results both in a data file and in postscript plots.

As part of this project, a Python visualization program was written to take an output file from the code and animate it into a video which may allow a better physical understanding of the energization process; this code may be obtained from the author. Using this tool and others that come with the RMF code, a variety of individual particle behaviors under RMF are observed. These behaviors are described in the following sections. All of these cases take place in a simulation modeled after the PFRC-2, with $r_s = 7$ cm, $\kappa = 4$, and an axial magnetic field of strength 1,000 Gauss. Other parameters are varied as described in each section.

3.5.1 Cyclotron orbits

The particle in 15 is in a cyclotron orbit confined to the midplane, starting from a position rfac = .5, zfac = 0, ϕ_0 =45° , and $\theta_0 = 90°$ and an energy of 5 eV. This orbit is shown in Figure 15.

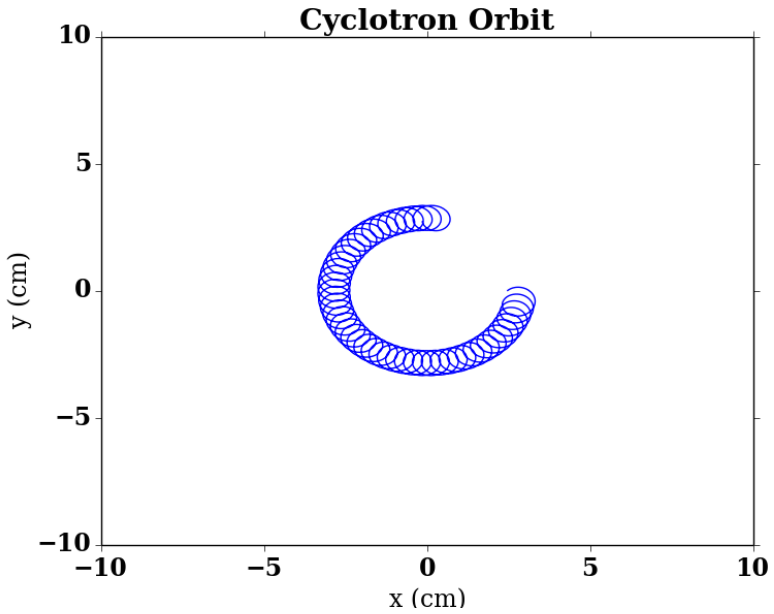

Figure 15: The cyclotron path of the particle examined in this section without RMF.

When RMF is applied to such cyclotron orbits, the nature of the result is strongly dependent on omfac (the frequency of the RMF in units of the ion cyclotron frequency at the center of the device) and the intial phase of the RMF. Consider, for example, an RMF of strength 25 G, frequency omfac = 1, and initial phase 45°. When this field is applied to the cyclotron orbit above, the ion gets pushed back and for by the RMF, but never obtains good heating. This orbit is animated in badcyclotron.mp4, which, like all subsequent videos, can be obtained from the author.

The energy of this orbit during the first 10 microseconds is shown in Figure 16. Clearly, the energy oscillates between nearly 0 eV and 20 eV, which is not the sort of behavior which would be good for heating to fusion-relevant temperatures. This type of behavior is characterized by the histogram shown in Figure 17, with two peaks on the ends.

The shape of the orbit bounces around in a way unsurprising given the oscillatory energy; this orbit path is shown in Figure 18.

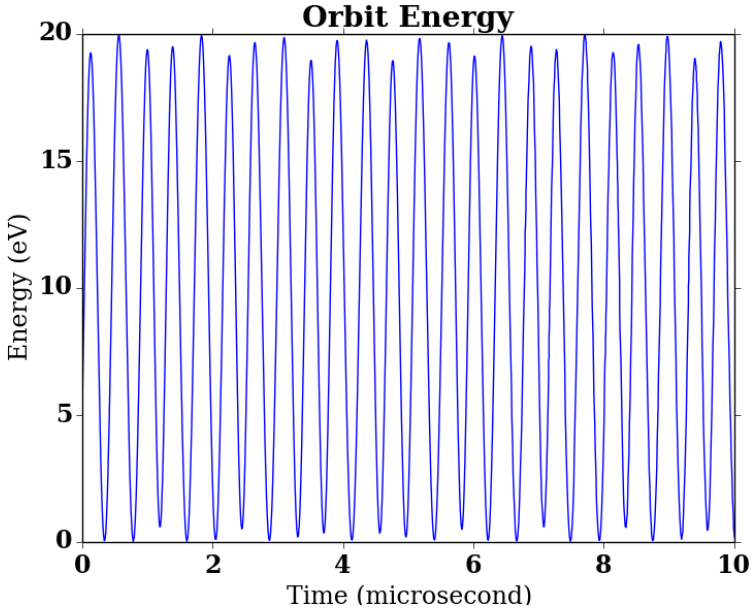

Figure 16: The energy of the cyclotron particle under RMF in a badly-heated situation

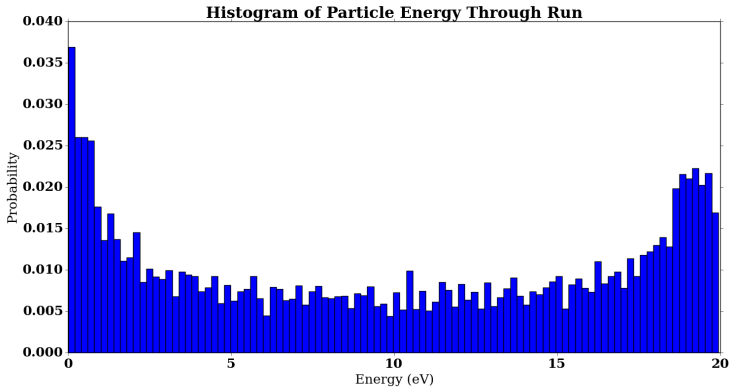

Figure 17: Histogram of badly heated orbit.

In some cases, however, the RMF can be made to align with this orbit in a way that allows it to obtain good heating. For example, if the phase of the RMF is changed to zero degrees, and the strength and the frequency of the RMF are left unchanged, the characteristics of the RMF are just right to knock the orbit into a more betatron-like shape, shown in Figure 19.

The energy of this orbit then increases in a much better way, shown in Figure 20. This orbit is animated in goodcyclotron.mp4. This type of energy change, which reaches large values, is characterized by the histogram in Figure 21: The particle spends the majority of its time at lower energies, but has occasional excursions to very high values.

To get some idea of how difficult it is for RMF to explosively heat a particle that is in the cyclotron orbit used in this section, Figure 22 shows the average energy of an ion during a 50 microsecond run versus the frequency and phase of the RMF. High heating is rare, and appears to require a precise combination of phase and frequency.

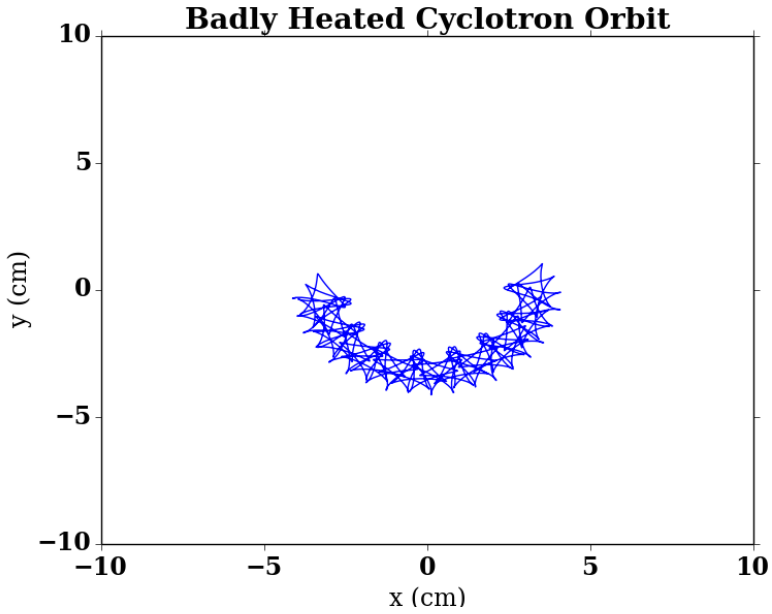

Figure 18: Path of badly heated cyclotron orbit.

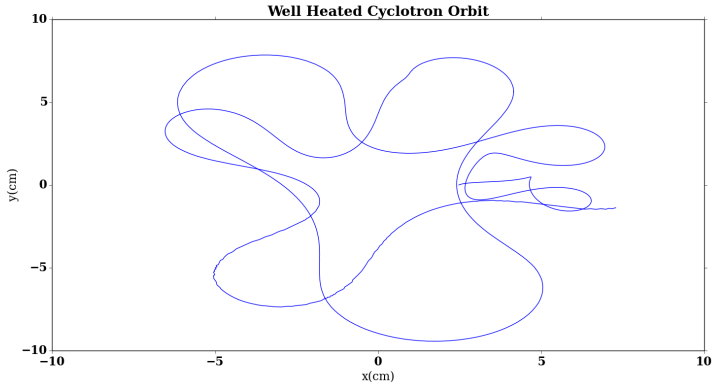

Figure 19: The path of the cyclotron particle when subjected to good RMF.

3.6 Betatron orbits

A similar analysis can be done with betatron orbits. The particle in 23 is in a betatron orbit confined to the midplane, starting from a position rfac = 1, zfac = 0, ϕ_0 =45° , and θ_0 = 90° and an energy of 5 eV. This orbit is shown in Figure 15.

When RMF is applied to such betatron orbits, the nature of the result is again dependent on omfac and the initial phase of the RMF, but betatron orbits are easier to heat than cyclotron orbits. Consider, for example, an RMF of strength 25 G, frequency omfac = 1, and initial phase 34°. This is one of comparatively few RMF fields which do not heat the ion well. The energy vs. time, histogram, and orbit path for this particle are shown in Figures 24, 25, and 26, respectively. This orbit is animated in badbetatron.mp4.

In many cases, however, betatron orbits are heated well: Unlike cyclotron orbits, they do not reverse direction quickly, allowing them to follow the rotating fields longer. An example

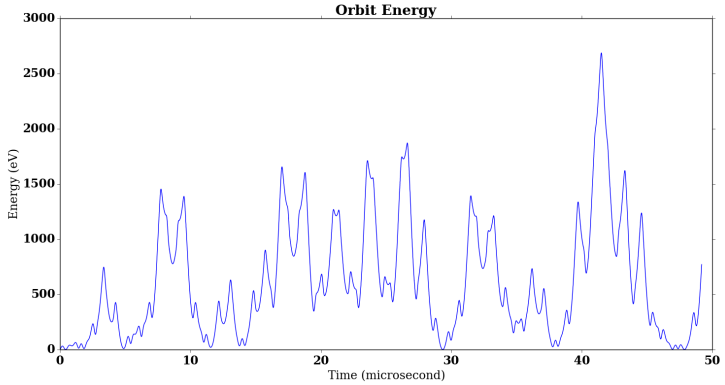

Figure 20: The evolution of the energy of a cyclotron orbit subjected to good RMF heating.

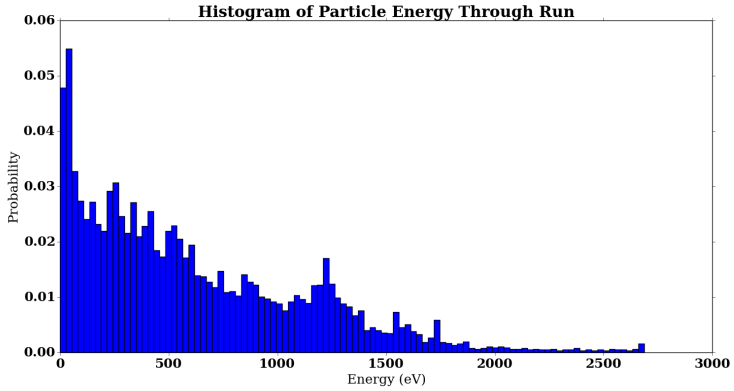

Figure 21

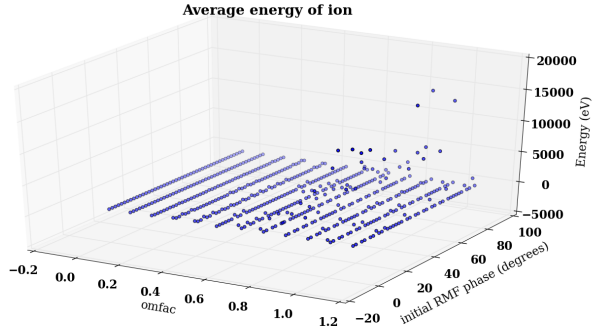

Figure 22: Average energy of cyclotron orbit over 50 microsecond run when hit with varying RMF parameters (if the particle escapes before the run is over, the average is computed over the time in which it is confined).

is described in Figures 27, 28, and 29. In this example, the particle enjoys great heating just before it escapes from confinement (note that the image of the path of the orbit only shows it at early time for clarity). This orbit is animated in goodbetatron.mp4.

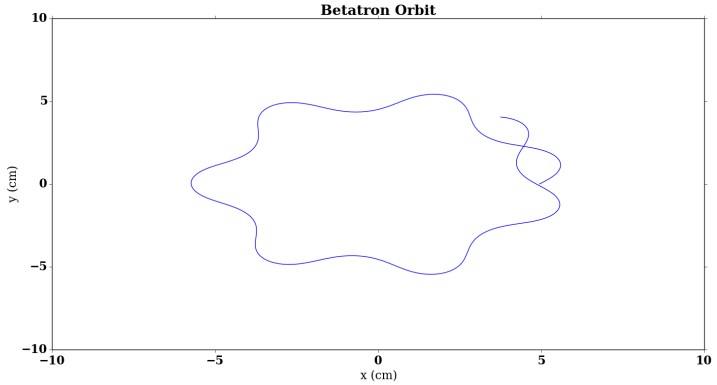

Figure 23: The betatron path of the particle examined in this section without RMF.

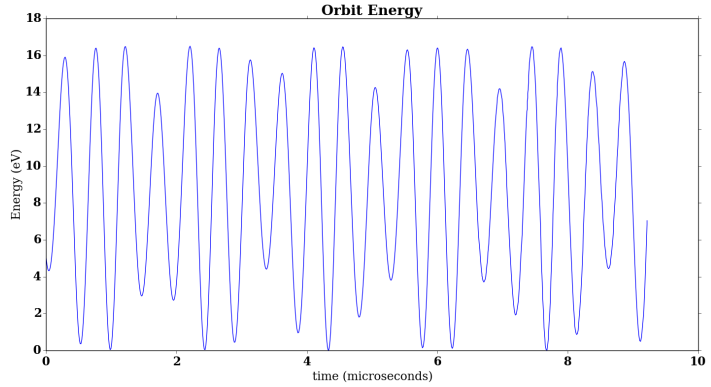

Figure 24: The energy of the betatron particle under RMF in a badly-heated situation

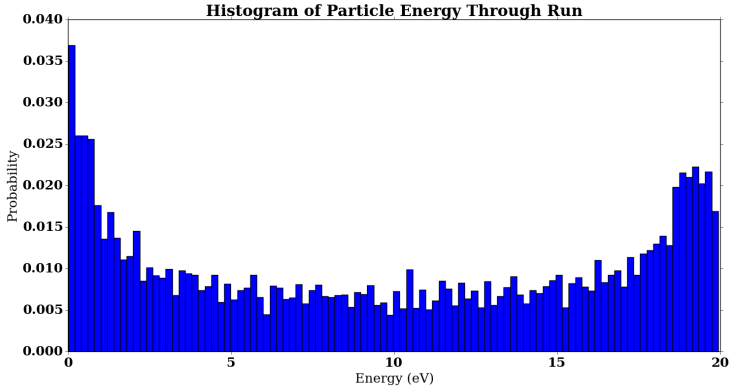

Figure 25: Histogram of badly heated orbit.

To see that it is indeed easier to get such heating for betatron orbits than for cyclotron orbits, a scan similar to that performed for the cyclotron orbit is performed for the betatron particle. The results are shown in Figure 30: Note that more combinations achieve significant energy gain than for the particle in the cyclotron position.

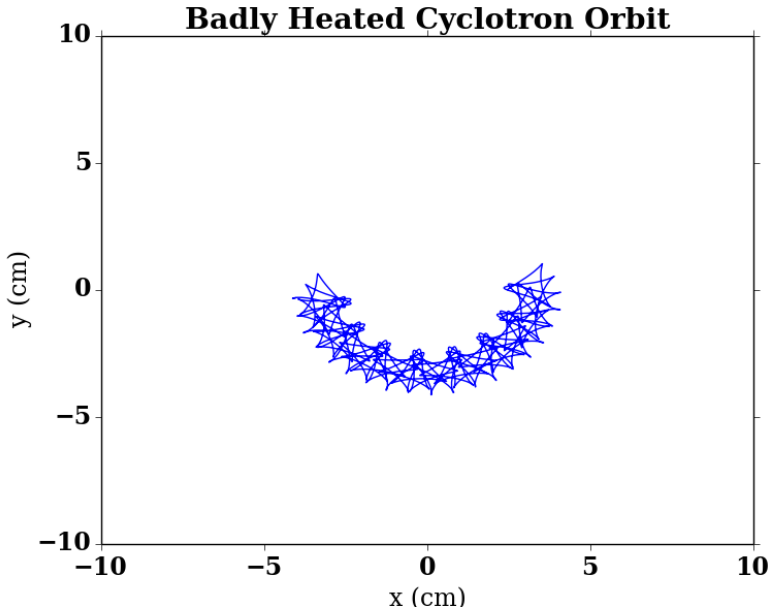

Figure 26: Path of badly heated betatron orbit.

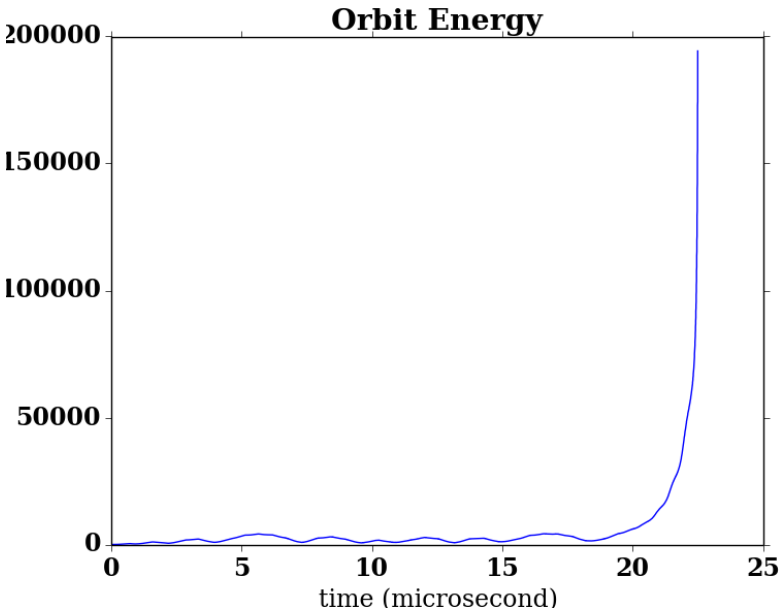

Figure 27: The evolution of the energy of a betatron orbit subjected to good RMF heating.

3.7 Figure 8 orbits

The heating of figure 8 orbits is treated in significant detail in [3], so an analysis is not repeated here. [3] finds that figure 8 orbits experience good heating overall which occurs at resonances of the RMF frequency with the frequency of the ion orbit.

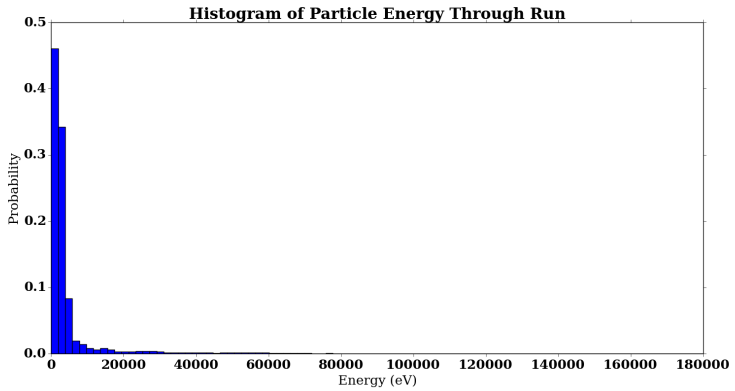

Figure 28: Histogram of betatron orbit that is heated well.

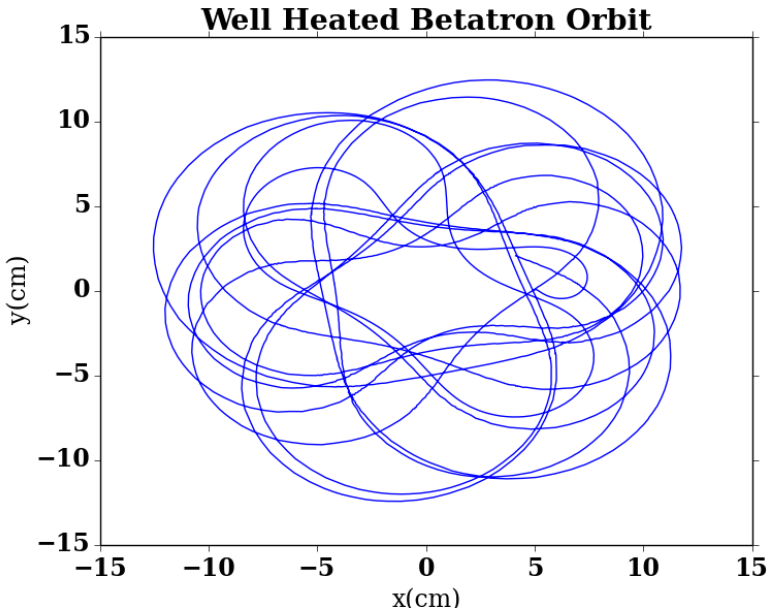

Figure 29: The path of the betatron particle when subjected to good RMF.

3.8 Analysis of ion response

The previous sections have presented a wide array of ion behavior, and these observations were limited to the midplane of the device. The variety of behavior that can be observed by taking a particle out of the midplane and also by varying the characteristics of the device is truly baffling.

Presented with such an array of behavior, gaining insight into ion behavior in a device as a whole is challenging. Landsman and Cohen have done many studies of ion behavior using careful analytic analysis of single ion paths; for example, the previously mentioned [3] models heated figure 8 orbits as perturbations on normal figure 8 orbits and finds various resonances that well describe the heating.

Future work might focus more on the properties of many different ions considered as a group. Particular emphasis could be placed on the distribution of particle energies in an FRC.

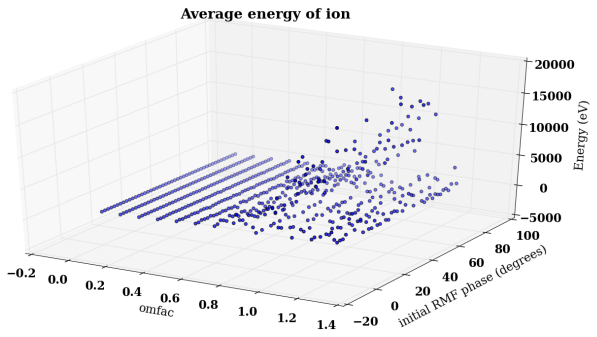

Figure 30: Average energy of betatron orbit over 50 microsecond run when hit with varying RMF parameters (if the particle escapes before the run is over, the average is computed over the time in which it is confined).

This is important: First, it is not the individual speeds of ions that matter but rather the speed of ions in relation to each other. If two ions move at a high velocity in the same direction, such behavior will not be good for fusion. Second, the shape of the distribution could influence how often fast ions lose their energy due to collisions with slower particles, a process which tends to relax a distribution towards a Maxwellian.

One concept which may also be enlightening in futures studies of FRC heating physics is entropy. The entropy of a distribution is defined as $\sigma = -\int f(v) \ln f(v) dv$. Since entropy can be related to heating, studying this quantity could be helpful towards understanding the overall heating behavior of the device. Entropy can also be a useful way of quantifying the difference between distributions of different shapes. For instance, the entropy calculated from distribution one of the slow distributions presented before, with two peaks, is smaller than the entropy of the distributions of particles that are heated well, with a tail on the end. Distributions with two peaks tend to have entropy around $\sigma \approx 3$, while distributions with a tail on the end tend to have entropy around $\sigma \approx 9$.

Finally, more research could be put into understanding how a particle explores phase space. Figure 31 contains dots representing the positions of a particle in a phase space composed of two components of its momentum. The blue dots show an orbit without RMF; the path in phase space is closed and predictable. When RMF is applied, the particle is kicked to higher energies, but it appears that a spot of similar shape to the original path remains unoccupied. Understanding better the nature of such apparently prohibited regions could help with a broader understanding of how RMF heats.

3.9 Limitations of single particle approach

The simulations presented thus far are for single particles not colliding with others. This model often works well in FRCs, because the plasmas are not extremely dense and the particle speed is often high enough to make particles unlikely to collide over the distance they travel in the device. However, Spitzer collisions involving electrons and ions will happen, and these collisions may tend to relax the distribution of particles in the FRC towards a Maxwellian equilibrium.

Another process relevant to the heating of ions, but ignored in this discussion, is charge exchange. In this process, an ion collides with a neutral particle and exchanges an electron

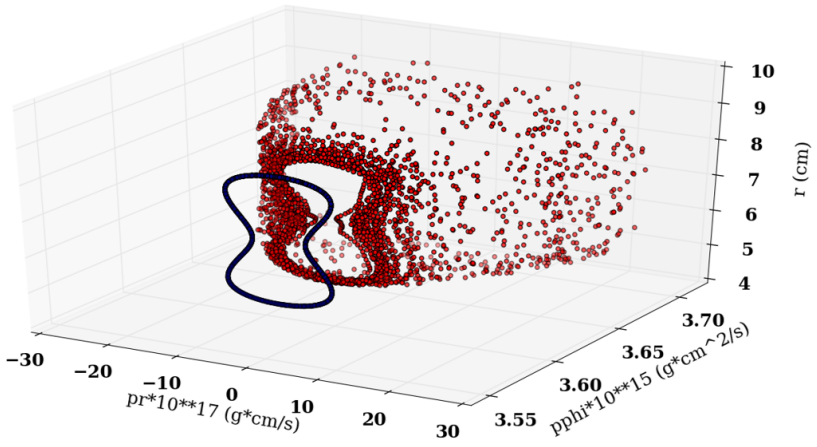

Figure 31: Dark blue points show locations in phase space for a figure 8 midplane orbit without RMF applied,r_s=10 cm, B_0 = 20,000 G ; red points show locations in phase space for the same orbit with an RMF field of amplitude 20 G and omfac = .95 applied

with it, so that the ion's energy is transfered to a neutral particle while an ion ends up with the energy of the neutral. This process is concerning, because the neutral, which is not confined by the magnetic field in the device, ends up with the energy in the ion, which is supposed to gain energy while remaining confined in the magnetic field so that it may fuse.

The PFRC is currently run with hydrogen gas. The total cross section for all hydrogen charge exchange reactions in hydrogen in the energy range at which the FRC is run is on the order of $\langle \sigma v \rangle \approx 10^{-7}$ cm^3 sec^{-1}. The rate of energy loss over the entire device would then be

$$P_{loss} = E_i \langle \sigma v \rangle n_n n_i V, \tag{16}$$

where V is the volume of the device, and and E_i is the energy of the ions. For ions of 1 keV in a device of volume 5,747 cm^3 (the volume of the confined region in the PFRC-2) with density $n_n = n_i = 10^{13}$ cm^{-3}, this loss rate is a very significant 5.747×10^{22} keV/sec = 9208 kW, more than the power available to heat the ions. It is thus important that the neutral density be lower than assumed here.

Finally, since preliminary simulations suggest that many ions may leave the confined region of the plasma during the course of their heating, the question of what happens to escaped particles is of central importance. This question is related to what happens to the neutral ions in the plasma. These neutrals may be ionized through collisions with plasma electrons; the rate of this ionization is described by $\frac{dn_0}{dt} = -n_0 n_e \langle \sigma v \rangle_{ionization}$, where n_0 is the neutral number density and n_e is the electron number density. This equation suggests that the population of neutrals in the FRC should decay with time. A decay of this form is not always observed. This suggests that perhaps a neutral flux is coming from the walls of the reactor under certain conditions; one possible source of this flux is the embedding of hot ions in the walls. If escaping ions came back as hot neutrals, they would not be useful to creating fusion reactions in the FRC unless the neutrals could again transfer their energy to the ions, perhaps via more collisions.

4 Ensemble response to RMF at different $B_{RMF}s$ and omfacs

We saw in the previous section that differently shaped orbits have different susceptibilities to heating. Though interesting, this fact does not alone answer how particles distributed through-

out a device would be heated. To attempt to provide insight into this question, this section presents results of simulations using large ensembles of particles evolved under varying RMF conditions. A particular goal of this work was to suggest regimes to be simulated by the more computation-intensive PIC code, which takes into account many of the factors described in 3.9.

4.1 Desirable conditions

In these simulations, the following conditions were desirable.

1. Ions reach high energy (about1 keV) in a timescale that can be simulated by computation-intensive PIC code (about 5 microseconds): 1 keV is the goal for ion heating in the current stage of the PFRC, while 5 microseconds requires a reasonable amount of computation.

2. RMF frequency as high as possible to allow for better current drive: Work in [6] suggests that higher frequencies tend to be better for RMF current drive, which is essential to creating the FRC confinement in the first place.

3. RMF field magnitude is limited by $\frac{B_{RMF}}{B_a} < .05$ to prevent field line opening and loss of confinement: RMF fields that are too large can destroy the Hill Vortex confinement structure, so care must be taken to avoid RMF fields that are too large.

4.2 Simulations

All of the simulations in this section used 2,880 particles. These particles all started with 5 eV, while their velocities were characterized by 12 values of the angle ϕ ranging between 0° and 330°, 5 values of the angle θ ranging between 30° and 150°. Their initial positions were distributed among 8 values of rfac from .1 to 1.5 and 6 values of zfac from 0 to 1.

4.2.1 B_0 = 1000 G

In the first set of simulations the background magnetic field was B_0 = 1,000 G. In addition, the parameter l, representing the periodicity of the RMF, was set to the value of $l = 1$. The average energy of the ensemble of ions at 5 microseconds is shown in Figure 34, while the fraction of ions that had escaped confinement at 5 microseconds is shown in Figure 35 (in the averages, particles leaving confinement were included at their last energy). As the diagrams demonstrate, under these conditions the ions had difficulty obtaining good heating under the timescales that PIC code could simulate, although they might see better heating on experimental timescales. This lack of good heating may in part be due to the large fraction of ions lost.

4.2.2 B_0 = 1500 G

In the second set of simulations, the background magnetic field was set to B_0 = 1,500 G, which was predicted to increase confinement, and the value of l was set to the value of $l = .5$, since this was believed to better represent the actual configuration in the FRC.

In this situation, the ions are able to obtain energies well in excess of 1 keV, even at relatively large omfacs like 2, which suggests PIC code should first work with situations having high axial magnetic fields. Interestingly, however, the fraction of ions lost is still high, despite the large confining field.

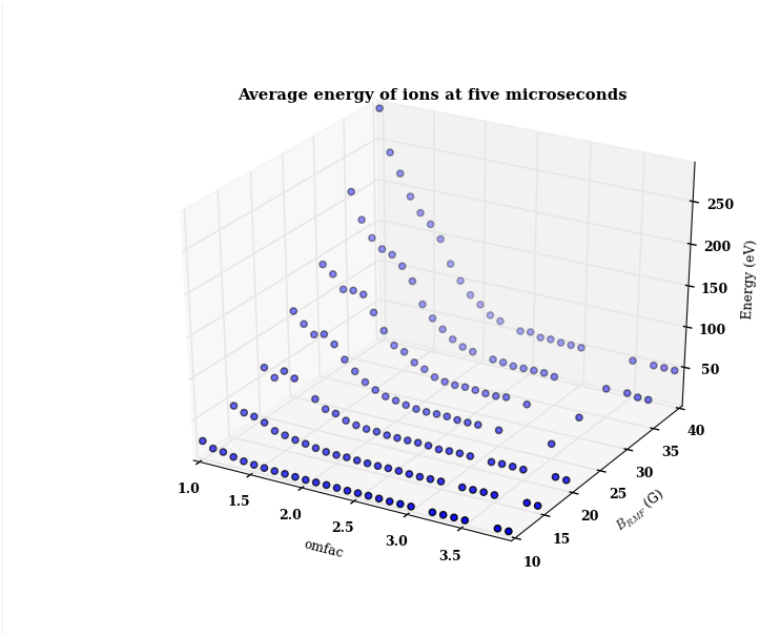

Figure 32: Average energy at 5 microseconds of ensemble of ions subjected to different RMF fields at $B_0 = 1{,}000$ G.

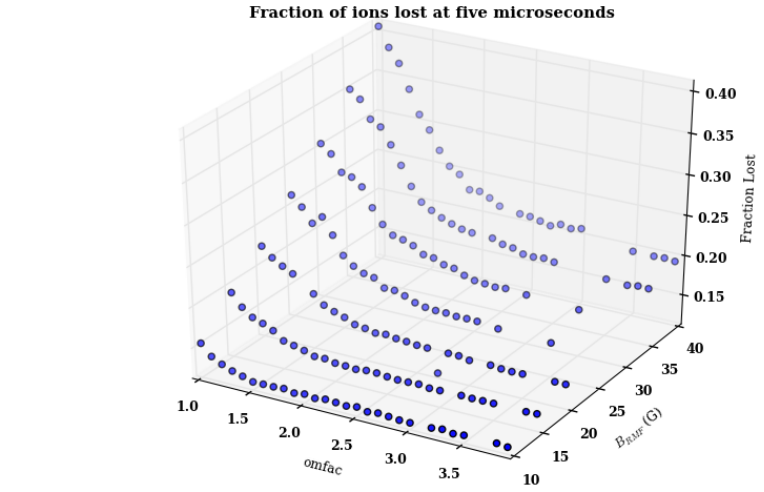

Figure 33: Fraction of ions lost at 5 microseconds under different RMF fields at at $B_0 = 1{,}000$.

5 Conclusion

This paper began with describing limiting characteristics of ion heating in the FRC as well as the experimental context in which such heating occurs from a macroscopic view. Then, it considered the microscopic specifics of FRC heating, including how different types of ion orbits

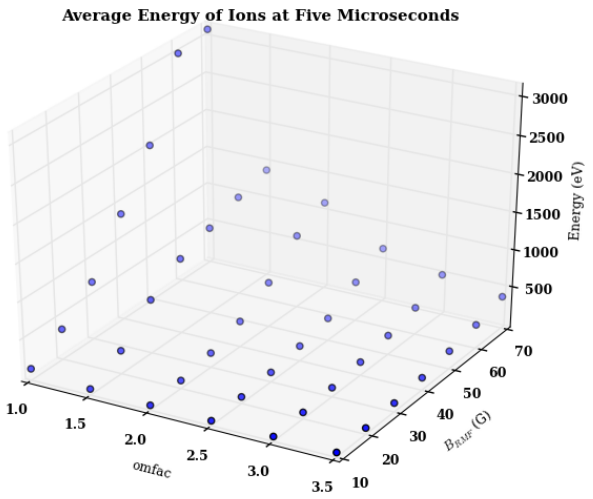

Figure 34: Average energy at 5 microseconds of ensemble of ions subjected to different RMF fields at $B_0 = 1{,}500$.

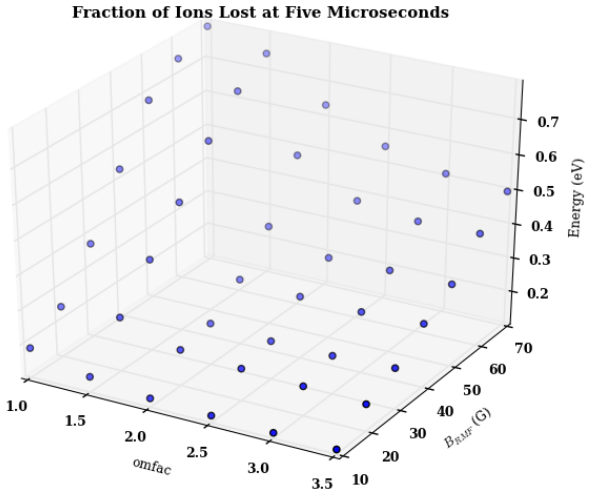

Figure 35: Fraction of ions lost at 5 microseconds under different RMF fields at $B_0 = 1{,}500$.

respond to the nature of the fields. In this section, it provided suggestions for areas of future research. Finally, it conducted ensemble simulations of ion response to RMF which suggest that PIC code simulations should use stronger values of B_0 for their work if they hope to obtain heating to 1 keV.

References

[1] C Brunkhorst, B Berlinger, N Ferraro, and SA Cohen. The princeton frc rotating-magnetic-field-experiment rf system. In *Fusion Engineering, 2007. SOFE 2007. 2007 IEEE 22nd Symposium on*, pages 1–4. IEEE, 2007.

[2] SA Cohen, B Berlinger, C Brunkhorst, A Brooks, N Ferraro, DP Lundberg, A Roach, and AH Glasser. Formation of collisionless high-β plasmas by odd-parity rotating magnetic fields. *Physical review letters*, 98(14):145002, 2007.

[3] SA Cohen, AS Landsman, and AH Glasser. Stochastic ion heating in a field-reversed configuration geometry by rotating magnetic fields. *Physics of plasmas*, 14(7):72508–72508, 2007.

[4] WN Hugrass and RC Grimm. A numerical study of the generation of an azimuthal current in a plasma cylinder using a transverse rotating magnetic field. *Journal of Plasma Physics*, 26(03):455–464, 1981.

[5] Alexandra Sasha Landsman, SA Cohen, and AH Glasser. Regular and stochastic orbits of ions in a highly prolate field-reversed configuration. *Physics of Plasmas (1994-present)*, 11(3):947–957, 2004.

[6] DR Welch, SA Cohen, TC Genoni, and AH Glasser. Formation of field-reversed-configuration plasma with punctuated-betatron-orbit electrons. *Physical review letters*, 105(1):015002, 2010.